Structural Characterization of Aldehyde-Terminated Self-Assembled Monolayers†

Alexandru Riposan, Yan Li, Yih Horng Tan, Giulia Galli, and Gang-yu Liu*

Department of Chemistry, University of California, Davis, California 95616

Received: August 1, 2007; In Final Form: October 9, 2007

The structure of aldehyde-terminated alkanethiol self-assembled monolayers (SAMs) on Au(111) is investigated using scanning tunneling microscopy (STM), atomic force microscopy (AFM), and density functional theory (DFT) calculations. For the first time, the structures of aldehyde-terminated SAMs are revealed with molecular resolution. SAMs of 11-mercapto-1-undecanal exhibit the basic $(\sqrt{3}\times\sqrt{3})$R30° periodicity and form various $c(4\times2)$ superstructures upon annealing. In conjunction with DFT studies, the models of the $(\sqrt{3}\times\sqrt{3})$R30° and the $c(4\times2)$ superstructures are constructed. In comparison with alkanethiol SAMs, the introduction of aldehyde-termini results in smaller domain size, lower degree of long-range order, large coverage of disordered areas, and higher density of missing molecules and other point defects within domains of closely packed molecules. The origin of these structural differences is mainly attributed to the strong dipole−dipole interactions among the aldehyde termini.

Introduction

Organic self-assembled monolayers[1] (SAMs) exhibit great potential for use in advanced applications ranging from biotechnology[2−5] to molecular electronics.[6−9] The ability to functionalize SAMs with a large variety of terminal groups allows the modification of surfaces to have tunable composition, reactivity, and physical properties such as hydrophilicity and lubricity. Furthermore, SAMs serve as excellent resists for nanofabrication, particularly in scanning probe-based nanolithography, for example, nanografting[3−5,10−14] and nanopen reader and writer.[15] Among their most important applications, functionalized SAMs are especially promising as the substrates for construction of chemical and bio-sensors.[16−18] For example, alkylthiol SAMs/Au(111) functionalized with hydroxyl (OH) termini provided a hydrophilic surface environment for bioapplications,[5] while carboxyl (COOH)[3,19] and aldehyde (CHO)[3,5] functionalities have been utilized as supports for protein immobilization via electrostatic and covalent interactions, respectively. The use of aldehyde termini has the advantage of forming strong covalent bonds with the primary amines in the protein residues.[20,21]

Despite many promising applications, aldehyde-terminated SAMs have not been characterized at molecular and nanoscopic levels. Knowledge of the molecular-level packing in the functionalized SAMs is critical in interfacial design for effective protein immobilization. For example, the dimension of proteins ranges from several to tens of nanometers; thus protein immobilization would likely depend upon the local domain structures at nanoscopic level. In addition to the technological needs, the characterization of the local structure of aldehyde-terminated SAMs is of scientific importance in determining the impact of the polar termini on the resulting SAMs' structures. It is known that the molecular packing of SAMs is influenced by the headgroup−substrate chemisorption, van der Waals (vdW) interactions among the backbones, and the interactions among the functional termini.[1] For *n*-alkanethiols SAMs, energetics are determined: 20−30 kcal/mol for the thiol-on-Au(111) chemisorption, ∼2 kcal/mol per CH_2 group for the van der Waals forces, and 2−8 kcal/mol per group for all other polar group interactions among polar termini.[1,22,23] These interactions result in closely packed molecular structures commensurate with the underlying Au(111) lattice. The most well-known lattice structures are a basic $(\sqrt{3}\times\sqrt{3})$R30° structure, as well as several $c(4\sqrt{3}\times2\sqrt{3})$R30°, or $c(4\times2)$, superlattices.[24−28] The conformation and orientation of the all-trans *n*-alkane chains in closely packed SAMs were revealed and quantified using three parameters: tilt (θ), rotation (χ), and twist (φ) angles for the molecular chains. As-deposited SAMs of methyl-terminated alkanethiols have $\theta = 30-40°$,[28−30] $\chi = 5-20°$ depending on chain length,[29] and $\varphi \approx 35-55°$ or $125-140°$ depending on the chain orientation and the hybridization status of the sulfur head group.[28,30−32]

The introduction of functional terminal groups is known to cause perturbation to the molecular-level packing. SAMs with OH and COOH termini exhibit a higher degree of disorder[22,33,34] and different (θ,χ,φ) chain orientation[22,32] from their methyl-terminated counterparts. Scanning tunneling microscopy (STM) revealed several ordered HO- and HOOC-terminated structures,[3,33−37] including the common $(\sqrt{3}\times\sqrt{3})$R30°[33] as well as other lattices like (3×12) and (3×3).[34,35,37] It was proposed that interactions among the polar termini and termini-water, for example, hydrogen bonding, may be responsible for the increase of disorder by disrupting the molecular-level close-packing.[22,34] The introduction of CHO termini differs from OH or COOH groups in that strong hydrogen bonds are unlikely to form among CHO groups, due to the fact that H atoms are not directly linked to strongly electronegative O atoms. On the other hand, water or solvent molecules in the media may form hydrogen bonds with the CHO termini during or after the SAM formation. Additionally, the dipole moment of CHO is stronger than those of OH and COOH, with estimated values of 2.72, 1.55, and 1.65 D, respectively.[38]

The impact of aldehyde termini to the molecular-level packing of SAMs is investigated in this work using STM and atomic force microscopy (AFM), in conjunction with density functional

† Part of the "Giacinto Scoles Festschrift".

* Corresponding author. E-mail: liu@chem.ucdavis.edu.

10.1021/jp076124g CCC: $37.00
Published on Web 12/06/2007

theory (DFT) calculations. SAMs of 11-mercapto-1-undecanal/Au(111), referred to herein as $C_{10}CHO$, were imaged and compared to the corresponding normal alkanethiol SAMs of undecanethiol, referred to herein as C_{11}, prepared under the same conditions. The $C_{10}CHO$ and C_{11} molecules have the same number of CH_2 groups in the alkyl chain, but are terminated with aldehyde (CHO) and methyl (CH_3) groups, respectively. Molecular resolution STM images attained from this investigation enable the determination of periodicity and chain packing. Combining our experimental results with DFT calculations, structural models are proposed for the closely packed structures. In addition, local domain structures at nanometer level are also clearly revealed, from which characteristic structural features of $C_{10}CHO$ SAMs are identified. New insight is provided regarding the local domain structures present in these SAMs.

Experimental Section

Preparation of SAMs. The Au(111) substrates were prepared by thermal evaporation of Au (Alfa Aesar, 99.999%) in a high-vacuum evaporator (Denton Vacuum, Inc., model 502-A) with a base pressure 3×10^{-7} Torr during evaporation. Typically, 200 nm gold films were deposited onto freshly cleaved mica (0001) surfaces (clear ruby muscovite, Mica New York Corp.), at a substrate temperature of 350 °C and a rate of 3 Å/s. Subsequently, the films were annealed in situ at 375 °C for 20 min, cooled to room temperature under vacuum, and hydrogen-flamed (99.99%, Praxair Inc.) upon removal from the deposition chamber. This procedure produced Au(111) terraces typically 100 nm wide.

Powder 11-mercapto-1-undecanal disulfide, $[S(CH_2)_{10}CHO]_2$, 99% purity, was purchased from ProChimia (Gdansk, Poland) and used without further treatment. The solutions were prepared by dissolving the compound in 99.99% purity ethanol (Gold Shield Chemical Co.) in clean glass jars (Fisher Scientific). Freshly prepared Au(111) substrates were immersed into 0.5 mM $[S(CH_2)_{10}CHO]_2$ solutions for at least 24 h at room temperature (296 K). The disulfide bonds likely dissociate at the gold surface, forming SAMs of $S(CH_2)_{10}CHO$.[39] Varying the solution concentration from 0.5 to 1 mM, or the immersion time from 24 h to 14 days, did not result in significant differences in the morphology of as-deposited SAMs, as observed in this STM and AFM study. For SAMs deposited at higher temperatures, the glass jars containing thiol solutions were preheated in an oven to the desired temperature prior to the immersion of the fresh Au(111) substrates. Upon typically 2 h immersion at the elevated temperature, the jars were removed from the oven and allowed to cool to room temperature for several hours. Upon the formation of the SAMs, the samples were removed from the solution and washed sequentially with ethanol, milli-Q water (18.3 MΩ), ethanol, hexanes (99.9%, Fisher Scientific), and ethanol, and briefly left to dry in air prior to transferring into the UHV-STM or the AFM microscopes. Undecanethiols (C_{11}) of 98% purity was purchased from Sigma Aldrich, and C_{11} SAMs were prepared following the same procedure as for the $C_{10}CHO$ SAMs.

STM and AFM Imaging. The STM studies were conducted under ultrahigh vacuum (UHV) in an RHK microscope (STM 100, RHK Technology, Inc.), at a base pressure below 5×10^{-10} Torr. For UHV annealing, a tungsten filament mounted underneath the sample stage provided thermo heating to designed temperature and duration. All samples were imaged at room temperature (~296 K) in constant-current mode, using tungsten tips prepared by electrochemical etching in 3 M KOH aqueous solutions.[40] Typical imaging conditions are: 0.2−1.5 V (both positive and negative biases) and 2−50 pA. We observed that the imaging conditions often became unstable during the STM of $C_{10}CHO$ SAMs, but not for C_{11} SAMs. The instability manifested into sudden oscillations in the tip−SAM distance, abrupt contrast changes or loss of resolution, and occasionally the disruption of the $C_{10}CHO$ SAM. The STM images reported in this Article were acquired in regions where the imaging conditions were stable, and no molecular desorption was observed during repeated scanning.

The AFM studies were conducted in a home-built scanner with a deflection-type configuration, controlled by RHK STM 1000 electronics. The SAMs were imaged in contact mode in ethanol media, using Si_3N_4 microlevers (Veeco Metrology Group, Santa Barbara, CA) with a force constant of 0.58 N/m. The typical imaging force used in this study ranged between 0.5 and 1 nN. To further investigate the regulation of the SAM domain structure, $C_{10}CHO$ nanopatterns were fabricated by AFM nanografting following a protocol developed previously.[10−12]

DFT Calculations. The calculations were performed using DFT in the Perdew−Burke−Ernzerhof generalized-gradient approximation (PBE/GGA)[41] and the Quantum-ESPRESSO package.[42] Norm-conserving pseudopotentials were employed, and wave functions were expanded in plane waves with a kinetic energy cutoff of 50 Ry. The Au(111) substrate was modeled with a repeated slab of four atomic layers with calculated bulk equilibrium lattice constant of 4.16 Å,[43] separated by nine layers of vacuum (~22 Å). For the regular $(\sqrt{3}\times\sqrt{3})R30°$ structure, a unit cell with three surface Au atoms and one adsorbate molecule was used and the Brillouin zone was sampled with a $6\times6\times1$ Monkhorst−Park (MP) k-point grid.[44] For the $c(4\times2)$ superstructure, a $p(3\times2\sqrt{3})$ unit cell with four adsorbate molecules was used, sampled with a $6\times3\times1$ MP grid. During structure optimization, the bottom Au layer was fixed while the top three Au layers and the adsorbed molecules were fully relaxed.

The $C_{n-1}CHO$ adsorption energy is defined as

$$mE_{ad} = E_{tot}[\mathrm{Au(111)}] + mE_{tot}[C_{n-1}CHO] - E_{tot}[C_{n-1}CHO/\mathrm{Au(111)}] \quad (1)$$

where $E_{tot}[C_{n-1}CHO/Au(111)]$, $E_{tot}[Au(111)]$, and $E_{tot}[C_{n-1}CHO]$ are the total energies of the $C_{n-1}CHO$/Au(111), a clean Au(111) surface, and a gas-phase $C_{n-1}CHO$ radical, respectively. m represents the number of adsorbate molecules per unit cell. Contributions to E_{ad} include both interactions between adsorbate molecules and the gold surface, E_{mol-Au}(chemisorption), and intermolecular interactions $E_{mol-mol}$(electrostatic, vdW, hydrogen bonding, etc.). Although vdW interactions are not fully captured at the GGA level, the DFT calculations are expected to provide reliable results for the relaxed geometries and electronic properties, because vdW interactions are small contributions to the total interaction energy for short and intermediate-length molecules ($n < 12$).

Results and Discussion

1. The Lateral Heterogeneity of $C_{10}CHO$ SAMs. $C_{10}CHO$ SAMs deposited at room temperature (296 K) were investigated under UHV using STM (Figure 1), and in EtOH using AFM (Figure 2). Figure 1a−c shows typical STM topographic images of $C_{10}CHO$ SAMs deposited at room temperature (296 K). For comparison, STM topographic images of the corresponding C_{11} SAM are shown in Figure 3. At first glance, the morphology of $C_{10}CHO$ (Figure 1a) exhibits similarities to that of C_{11} (Figure 3a), both containing closely packed domains, etch pits, and

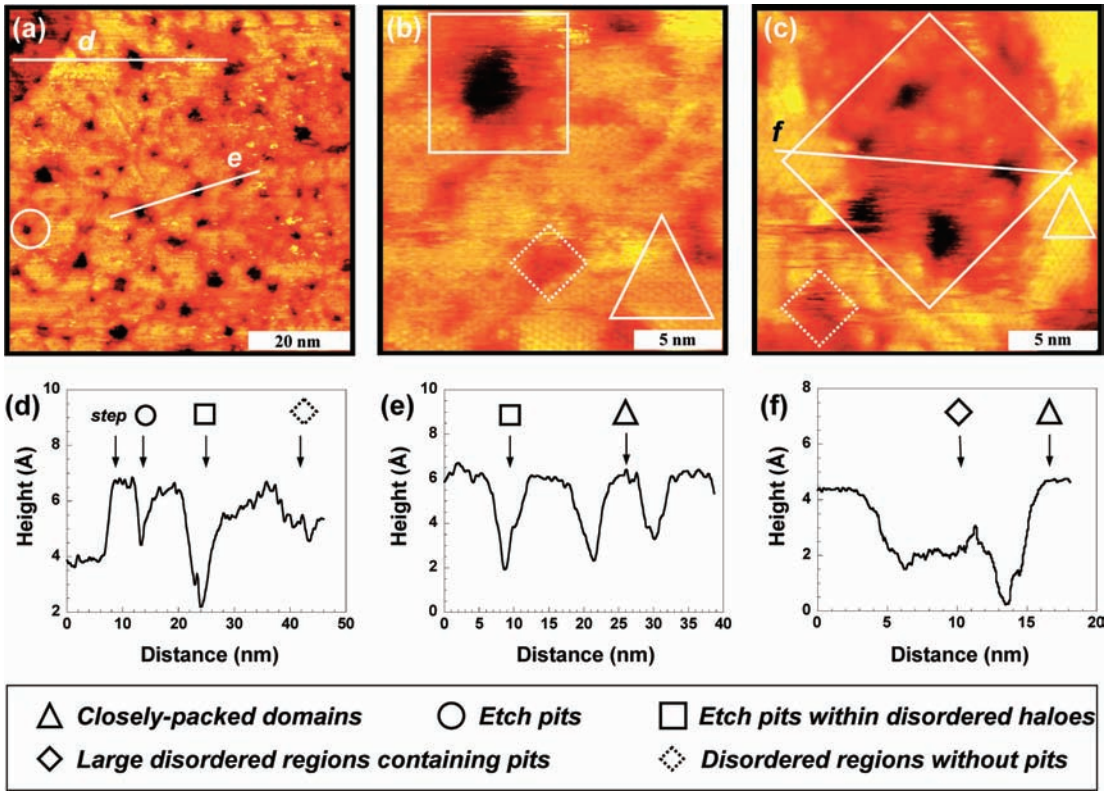

Figure 1. (a) STM topographic image illustrating the typical morphology of C_{10}CHO SAMs formed at 296 K. Characteristic topographic features are indicated with discrete symbols in the legend, which will be consistently used through the Article. Areas containing closely packed domains and large disordered regions are shown at higher magnification in (b) and (c), respectively. The images were acquired at (a) (0.8 V, 23 pA), (b) (0.8 V, 17 pA), and (c) (1.0 V, 17 pA). (d−f) Height profiles corresponding to the lines marked *d*, *e*, and *f*, respectively, in (a) and (c).

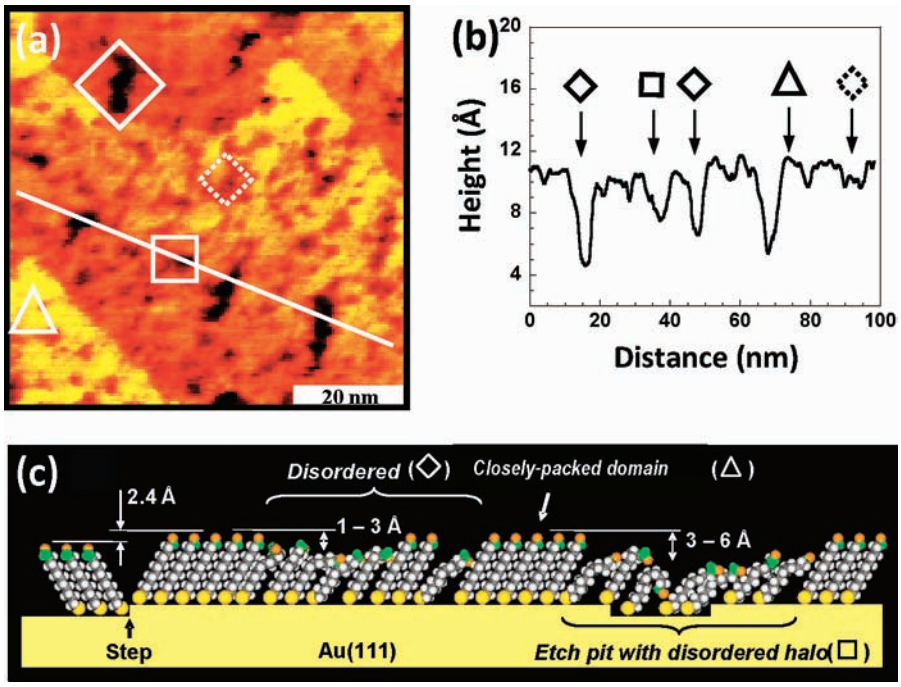

Figure 2. (a) AFM topographic image of a C_{10}CHO SAM formed at 296 K. (b) True height corrugation along the line marked in panel (a). (c) Schematic diagram illustrating the disordered structure of as-deposited C_{10}CHO SAMs. The CHO termini are represented in green (C and H) and orange (O) for each molecule.

domain boundaries.[40] Further review of STM topograph reveals three new morphological features associated with C_{10}CHO SAMs: (i) etch pits surrounded by disordered haloes (indicated by solid squares), (ii) disordered regions (indicated by broken diamonds), and (iii) disordered areas containing pits (indicated by solid diamonds). The size of closely packed C_{10}CHO domains typically ranges from 2 to 8 nm, smaller than that for C_{11} SAMs (Figures 1 and 3). As quantified by the cursor profiles shown in Figure 1d−f, the disordered C_{10}CHO regions are 2−15 nm in width with an apparent height of 0.1−0.3 nm smaller than that of the closely packed domains. The etch pits themselves are 1−4 nm in diameter and are usually surrounded by haloes

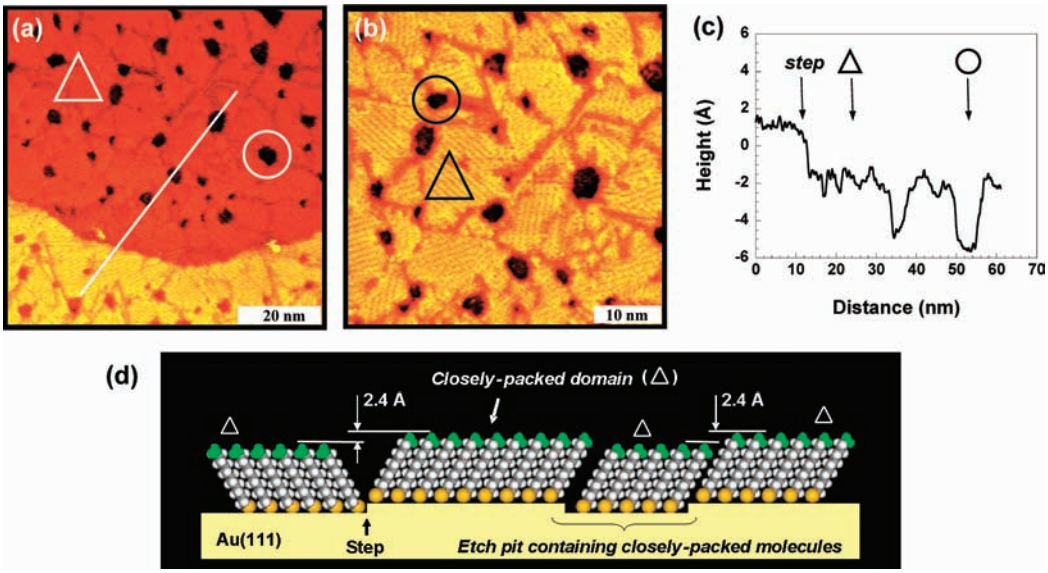

Figure 3. (a and b) STM topographic images illustrating the typical morphology of C_{11} SAMs formed at 296 K. The images were acquired at (a) (1.0 V, 19 pA), and (b) (1.0 V, 22 pA). (c) Height profile corresponding to the line marked in panel (a). (d) Schematic diagram illustrating the well-ordered structure of as-deposited C_{11} SAMs.

of disordered molecules, extending up to several nanometers outward. The apparent depth of the surface pits is 0.25−0.55 nm, larger than the height of a single atomic Au(111) step (0.235 nm) (Figure 1d). This further confirms the disorder among the C_{10}CHO molecules inside and outside the pits. The presence of disordered regions observed for C_{10}CHO SAMs is similar to those observed previously for mercaptohexanol (C_6OH) SAMs formed in UHV.[34]

The presence of disordered regions in C_{10}CHO SAMs is also consistent with the AFM investigation, where the disordered areas appear as dark contrasts in the AFM topograph shown in Figure 2. Unlike STM, where the apparent height is a convolution of physical height and local density of states (LDOS),[26] AFM enables measurement of true height.[45] For as-deposited SAMs, AFM reveals closely packed domains of 2−10 nm in size, separated by a high density of dark depressions with depth ranging from 0.2 to 0.6 nm, from the cursor profiles (e.g., in Figure 2b). This depth is larger than that of the etch pits (0.24 nm) seen from AFM images of alkanethiols,[11] and thus is attributed to the presence of disorder most likely due to the lower coverage than in closely packed SAMs. For soft materials such as SAMs, deformation may be estimated from AFM topographic scans and the value of the load, following simple Hertzian mechanics.[45,46] Closely packed regions would exhibit lower deformation than the low coverage or defective areas. The difference in deformation manifests into depression in AFM topograph for domain boundaries and low coverage areas. Schematically, the packing/disorder of aldehyde SAMs is shown in the model in Figure 2c.

The high degree of disorder of C_{10}CHO is not observed for methyl-terminated SAMs formed under similar conditions.[24,25,27,40,47] As a comparison, the C_{11} SAM shown in Figure 3 is composed of closely packed domains 5−15 nm wide, separated by narrow domain boundaries. Large disordered regions, as those observed for C_{10}CHO SAMs (Figure 1c), are not present in C_{11} SAMs. The etch pits in C_{11} SAMs measure up to 6 nm in width and do not display wide and disordered haloes. All pits are 0.25−0.30 nm deep (Figure 3c), corresponding well with the single atomic Au(111) step height. The model shown in Figure 3d illustrates the structure of C_{11} SAMs where molecules are closely packed and faithfully decorate the Au surfaces, including the surface defect areas such as pits.

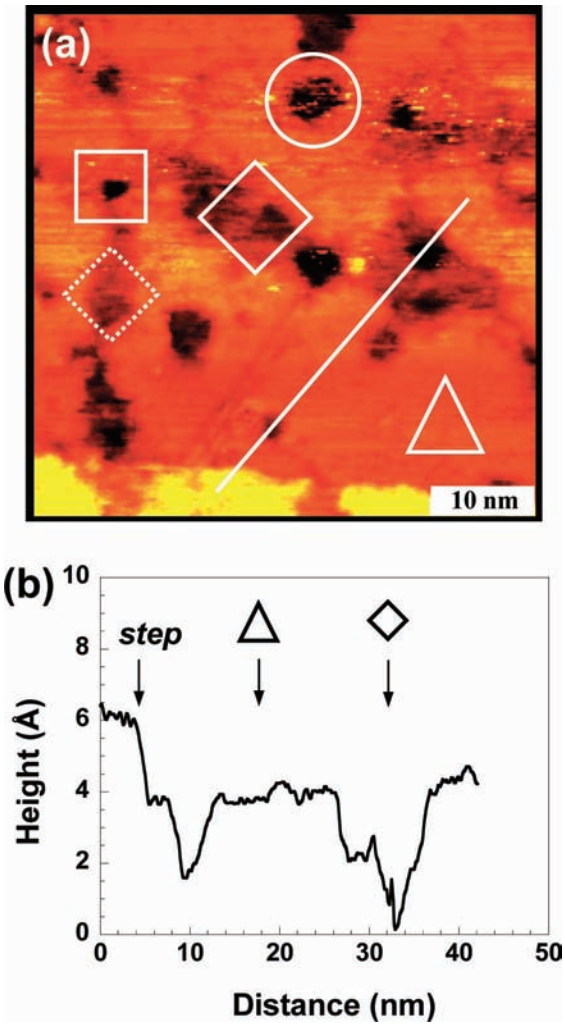

Figure 4. (a) STM topographic image illustrating the typical morphology of C_{10}CHO SAMs formed at 340 K for 2 h from 0.5 mM ethanol solutions. The image was acquired at (0.8 V, 11 pA). (b) Height profile corresponding to the line marked in (a).

2. Probing the Origin of Morphological Heterogeneity of C_{10}CHO SAMs. The fact that disordered regions are present

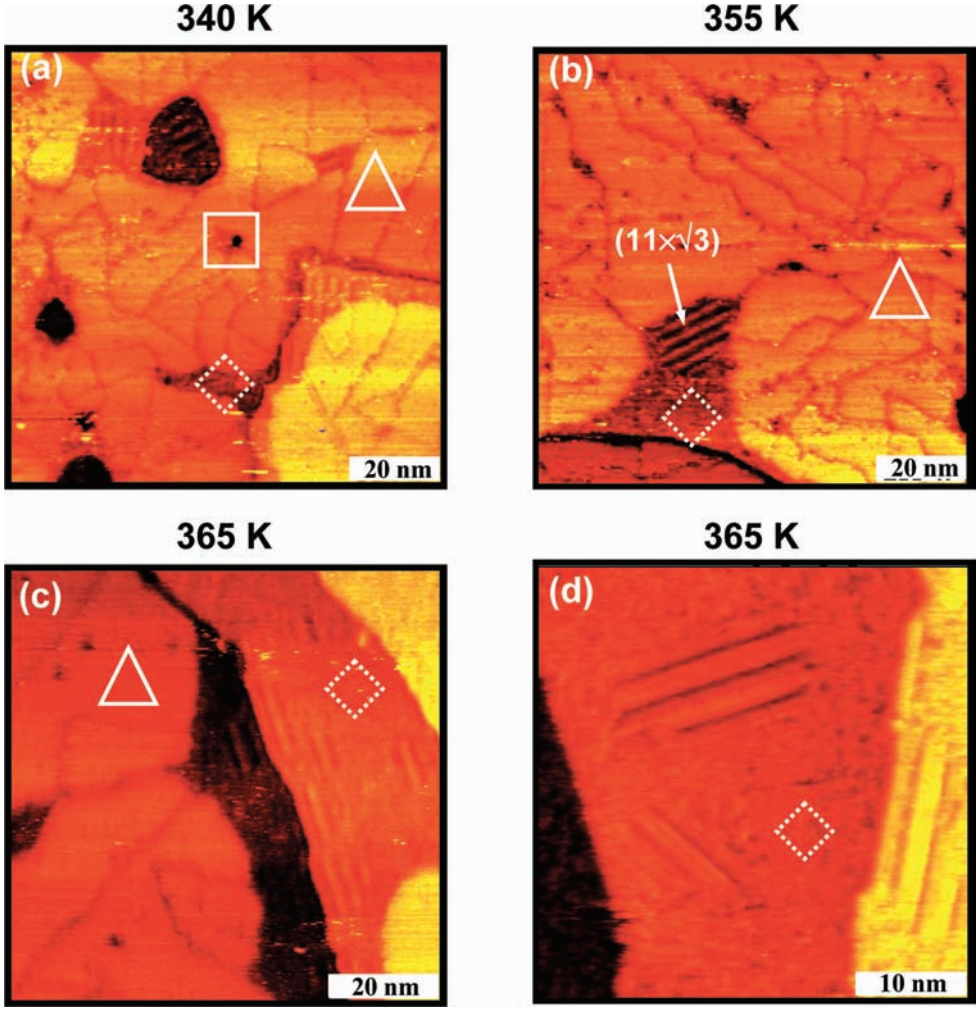

Figure 5. STM topographic images illustrating the evolution of C_{10}CHO SAMs during UHV annealing for 4−7 h at the temperatures indicated. Small domains of striped phases are indicated by their $(11\times\sqrt{3})$ symmetry. The images were acquired at (a) (1.3 V, 20 pA), (b) (1.2 V, 22 pA), (c) (0.8 V, 14 pA), and (d) (0.4 V, 5 pA).

when imaged under UHV suggests the importance of CHO dipole−dipole interactions. DFT calculations indicated that the CHO group can rotate relatively easily in the gas phase, with a barrier of approximately 1 kcal/mol between energy minima. However, once the molecules are arranged into a closely packed SAM, the strong dipole−dipole interaction introduces a CHO terminus rotation such that the C═O double bond lies nearly parallel to the surface. Using a dipole moment of 2.72 D for the CHO group[38] and the nearest neighbor (NN) distance of 5.0 Å, the energy difference of NN dipole−dipole interaction was calculated to be about 3.8 kcal/mol in the case of CHO pointing-up with respect to lying-down. The locality of dipole contribution was explored by including next NN (4.6 kcal/mol), third NN (5.1 kcal/mol), and up to the 10th NN, or 6.6 kcal/mol. Because of its short-range nature (∼third NN), such interactions provide sufficient barrier to "lock in" the local dipoles among neighbors. During the formation of SAMs, this locality hinders the movement and reorientation of the adsorbate molecules and restricts the forming of large domains of closely packed molecules, that is, the long-range order.

The effect of water or CHO−water hydrogen bonding was investigated by comparing UHV STM images with solution-phase AFM topography. The coverages of disorder observed in UHV using STM [Figure 1a] and in ethanol using AFM [Figure 2a] measure approximately 34% and 38%, respectively. Because of the tip-convolution, the value from AFM is an underestimation. Thus, these SAMs in ethanol exhibit a slightly higher degree of disorder than those observed in UHV. The difference is likely due to additional termini-ethanol or termini-water hydrogen bonding at the SAM surfaces when imaging in EtOH. Direct hydrogen bonding among aldehyde termini is expected to be weaker than among carboxyl or hydroxyl groups.[48] Nevertheless, ethanol or water molecules in the solvent may form hydrogen bonds with the O atoms at the termini. Our observation is similar to previous work, where random hydrogen bonding formed during the early stages of growth caused disorder in carboxylic acid-terminated SAMs.[22] Analogous behavior was reported for HO-terminated SAMs, where water adsorbed on preformed hydrophilic SAMs thus induced structural disorder within ordered domains by altering their molecular-level packing.[34] A high degree of disorder at the surface of closely packed hydrophilic SAMs, caused by the adsorption of water or solvent molecules, was also predicted by molecular dynamics simulations.[49]

The importance of inter-CHO interactions was further revealed through introduction of various perturbations to the structure of aldehyde SAMs. First, the reaction temperature was elevated to increase the surface mobility of the adsorbate molecules, which facilitates molecular ordering and the formation of energetically stable structures.[19,26,40] Second, SAMs were annealed in UHV to investigate the mobility of adsorbates.

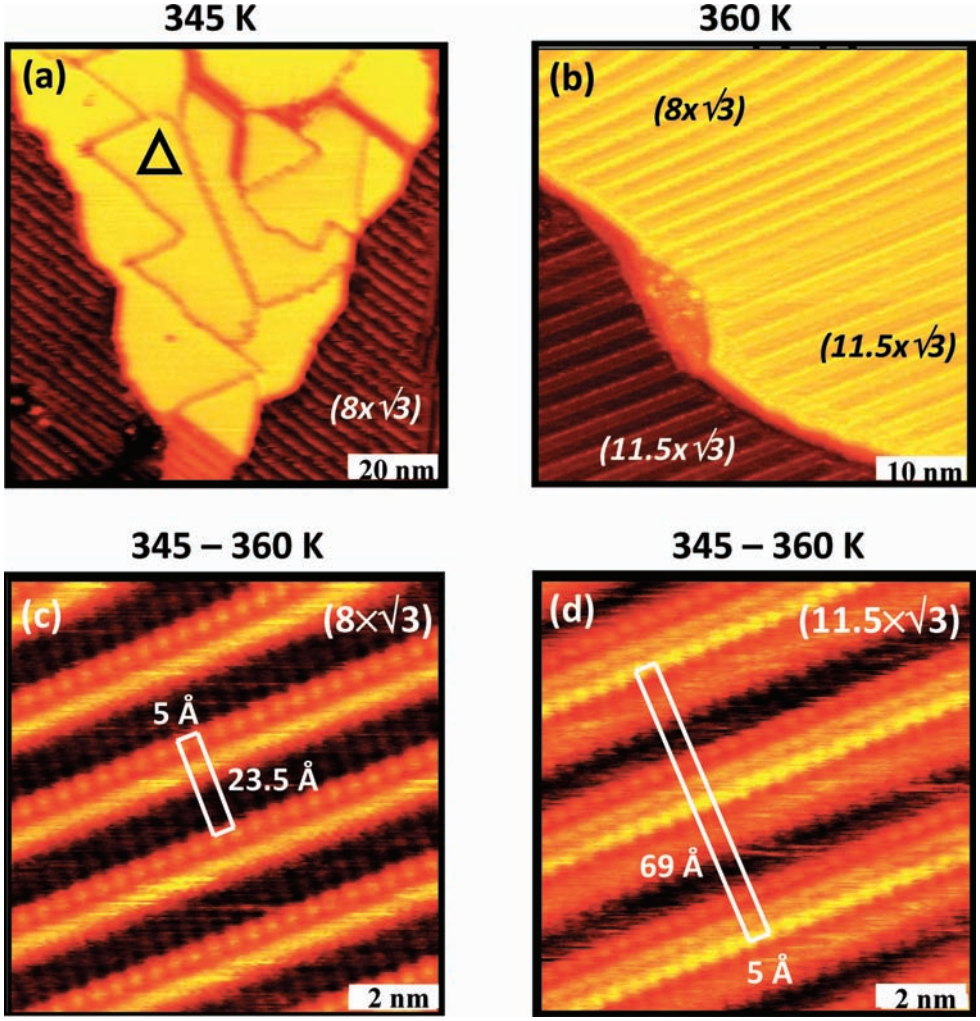

Figure 6. STM topographic images illustrating the evolution of C_{11} SAMs during UHV annealing for 4−6 h at the temperatures indicated. The closely packed domains are indicated with triangular symbols. Large domains of stripe phases with long-range order are indicated by their $(8\times\sqrt{3})$ and $(11.5\times\sqrt{3})$ symmetries, together with the unit cells and characteristic spacing. The images were acquired at (a) (0.8 V, 11 pA), (b) (0.8 V, 10 pA), (c) (0.8 V, 2 pA), and (d) (0.6 V, 2 pA).

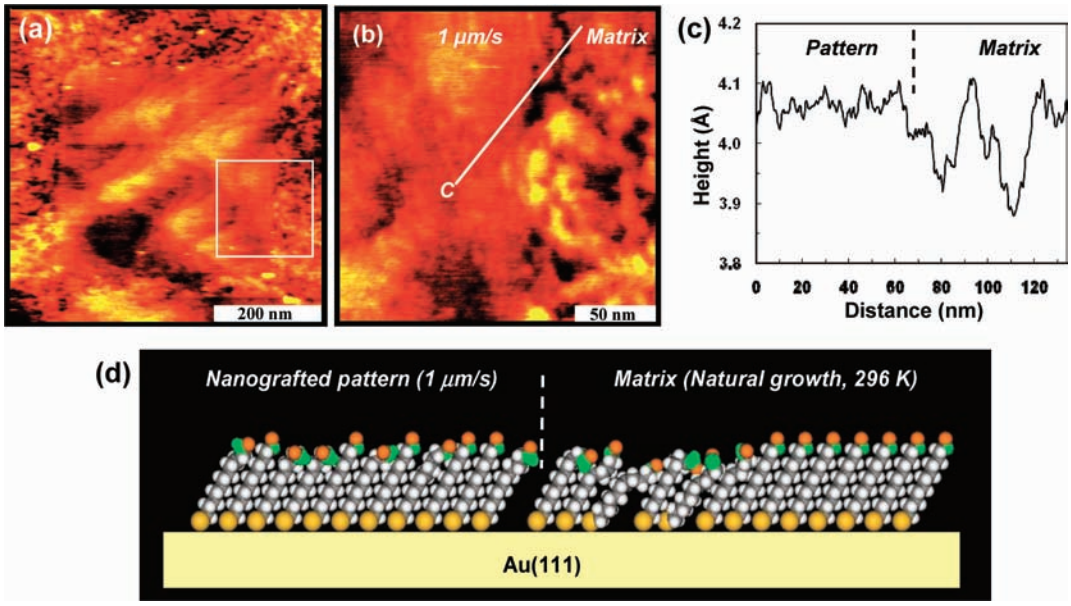

Figure 7. (a) AFM topograph showing a 400 × 400 nm^2 $C_{10}CHO$ nanopattern fabricated by AFM-based nanografting in a $C_{10}CHO$ matrix SAM. The matrix SAM was formed by natural growth at 296 K. (b) Zoom-in of the area marked by a square in (a). The image shows clearly the different morphology in the nanopatterned area (left) and the matrix SAM (right). (c) True height profile along the line marked *C* in panel (b). (d) Schematic diagram illustrating the different morphology in the nanopatterned area (left) and the matrix SAM (right).

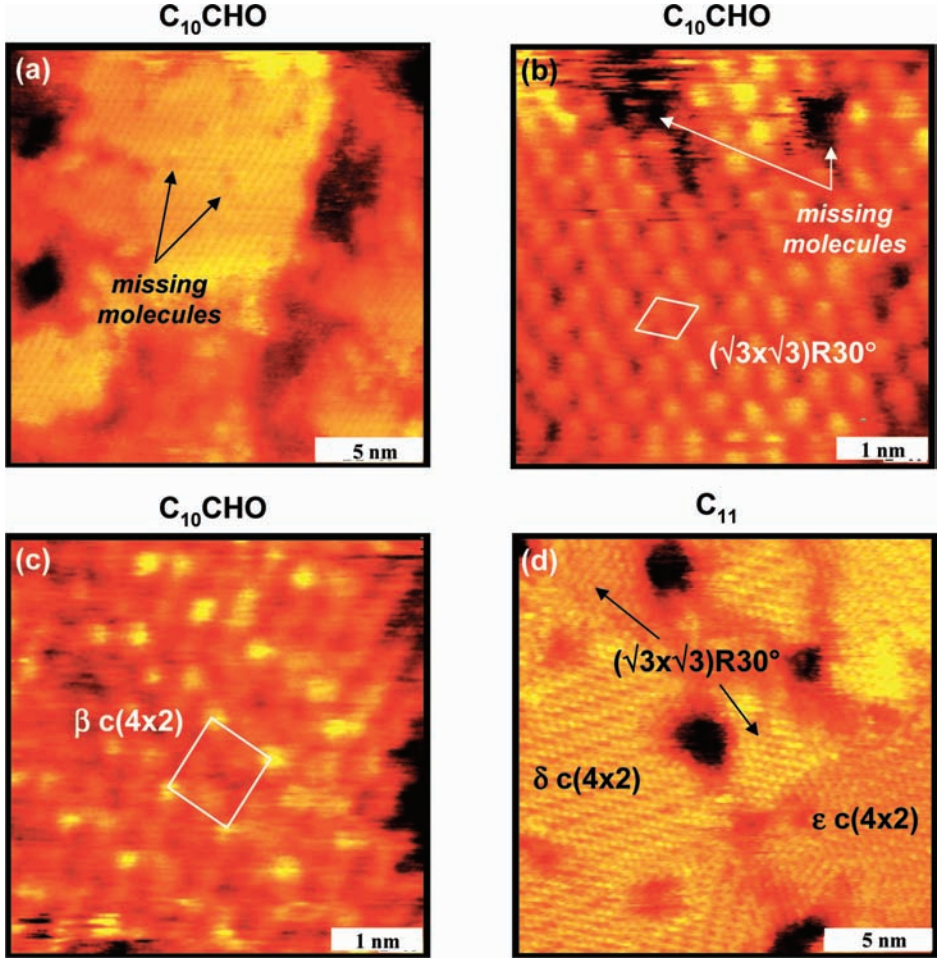

Figure 8. (a−c) High-resolution STM topographic images of $C_{10}CHO$ SAMs formed at 296 K. The closely packed domains display almost exclusively the $(\sqrt{3}\times\sqrt{3})R30°$ periodicity (a,b), but small domains of $c(4\times2)$ are also observed (c). (d) STM topographic image of a C_{11} SAM formed at 296 K. In comparison to $C_{10}CHO$, the C_{11} exhibits a higher degree of order and a higher coverage of $c(4 \times 2)$ superstructures. The type of periodicity, the corresponding unit cells, and point defects are indicated in the figure. The images were acquired at (a) (1.0 V, 18 pA), (b) (1.0 V, 10 pA), (c) (1.0 V, 11 pA), and (d) (0.8 V, 20 pA).

Finally, AFM-based nanografting was utilized to attain more kinetics-driven domain structures.[13,14,50]

2.1. The Lateral Heterogeneity of $C_{10}CHO$ SAMs Formed at Elevated Temperatures. Increasing reaction temperature changes the surface morphology of SAMs. This is exemplified in Figure 4a, which shows an STM topograph acquired under UHV, for the $C_{10}CHO$ SAMs formed from solution deposition at 340 K for 2 h. Figure 4b shows the height profile as indicated in Figure 4a. The size of ordered domains is increased from <10 nm at 296 K to 30 nm at 340 K. The size increase of ordered domain is consistent with an increased surface mobility, similar to CH_3- and HOOC-terminated SAMs.[19,40,51] Fewer but larger pits are observed, up to 6 nm in diameter. The coalescence of etch pits is also similar to the observations of those in alkanethiol SAMs, which was attributed to the movement of gold atoms at the top layer.[40,52] The disordered regions are still present, with larger size than that formed at room temperature, most likely due to coalescence of disordered domains. This coalescence, however, indicates that the degree of surface mobility in those areas is not sufficient for molecular packing and long-range ordering. These observations further suggest that the local interactions among aldehyde thiols are stronger than those of the corresponding *n*-alkanethiols such as C_{11} or C_{12}.

2.2. The Lateral Heterogeneity of UHV-Annealed SAMs. The heterogeneity of $C_{10}CHO$ SAMs is reduced upon UHV annealing. Heating in UHV facilitates the movement of molecules, and it provides relatively water-free SAM termini, as compared to the SAMs in ambient or solution phases. Figure 5 shows STM topographs acquired at three characteristic annealing temperatures. Upon annealing to 340 K, the typical domain size ranges between 10 and 25 nm, accompanied by coalescence of pits and disordered domains. Ordered domains became ~40 nm upon annealing at 365 K. As a direct comparison, the UHV annealing of C_{11} thiols is shown in Figure 6. A similar trend of increase in domain size is evident, with a much higher degree of long-range order (>60 nm at 345 K) than the aldehyde SAMs. The improvement of order in both cases is enthalpic with the facilitation of the movement of the molecules and the reorientation of chains, respectively.

Different from the annealing of C_{11} SAMs, or CH_3-terminated alkanethiols in general,[47,53] annealing for longer durations, for example, 10 h at 365 K, did not result in an improvement in long-range ordering; instead, the SAMs exhibited large disordered areas (Figure 5d), presumably of low coverage. In addition, increasing annealing temperature, for example, to 380 K, resulted in significant molecular desorption. The remaining thiol molecules formed small domains of striped phases (<20 nm), instead of long-range ordering of striped structures. The striped structures are ordered low-coverage phases, which form upon the annealing of closely packed alkanethiols due to molecular desorption.[47,53] Most $C_{10}CHO$ stripes observed were spaced at approximately 3.2 nm, corresponding to a $(11\times\sqrt{3})$

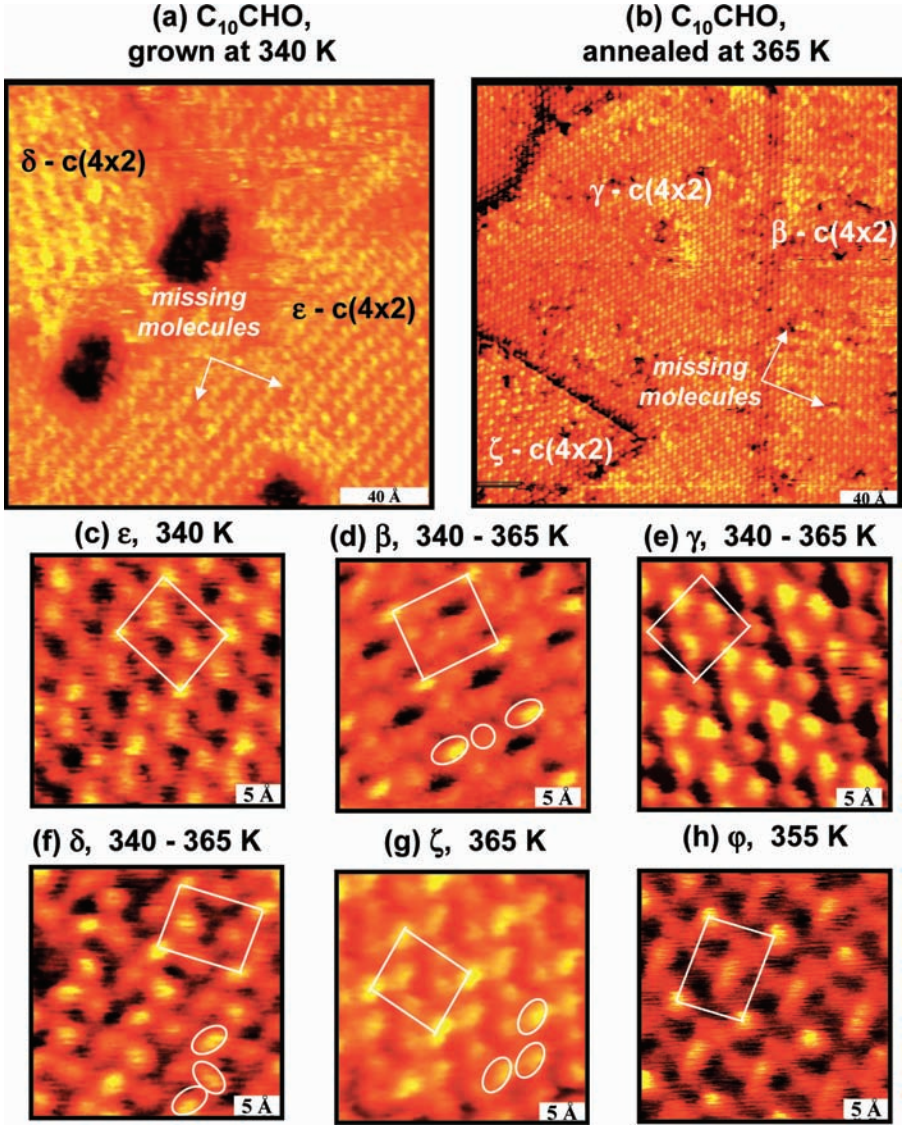

Figure 9. High-resolution STM topographic images of C_{10}CHO SAMs, (a) formed at 340 K, and (b) formed at 296 K and UHV-annealed at 365 K. Adjacent domains of various $c(4\times2)$ superstructures are observed. (c−h) High-resolution STM topographs showing a summary of the $c(4\times2)$ C_{10}CHO structures observed after annealing at the temperature ranges indicated. The type of periodicity, the corresponding unit cells, and SAM defects are indicated in the figure. The images were acquired at (a) (0.8 V, 8 pA), (b) (0.8 V, 19 pA), (c) (0.8 V, 11 pA), (d) (1.3 V, 24 pA), (e) (0.8 V, 17 pA), (f) (0.3 V, 6 pA), (g) (0.8 V, 19 pA), and (h) (0.3 V, 5 pA).

structure.[47,53−55] For comparison, Figure 6 shows the evolution of C_{11} SAMs upon UHV annealing in a similar temperature range. Mild annealing (345 K) of C_{11} SAMs leads to a significant increase in domain size of closely packed structures (40 nm). Annealing C_{11} SAMs at higher temperature preserves the long-range order and results in the intermixing of two types of ordered structures, large domains of closely packed molecules (>60 nm) and striped phases (>70 nm), consistent with previous observations for other alkanethiols.[47,53−55] The two C_{11} striped phases observed have inter-stripe spacing of 2.35 ± 0.03 and 3.29 ± 0.03 nm, corresponding to $(8\times\sqrt{3})$ and $(11.5\times\sqrt{3})$ structures, respectively. These phases correspond to the $(7.5\times\sqrt{3})$ and $(11.5\times\sqrt{3})$ structures reported previously for decanethiol (C_{10}) SAMs.[47,55]

The similarity and differences of the two SAMs underline the importance and strength of the local interactions among aldehyde termini. The local interaction hinders the long-range ordering of closely packed domains in a UHV environment. In addition, stripe phases exhibiting long-range order have been reported only rarely for OH-terminated alkanethiols, where the dipole is weaker than for aldehyde.[56] As discussed earlier, DFT calculations suggest that the strong dipole−dipole interactions among neighboring CHO groups are mainly responsible for the presence of disordered areas for as grown and high coverage SAMs. This evidence collectively suggests that these dipole interactions are likely the cause for the lack of long-range order at the low coverages, that is, lacking of large areas of striped phases. Other intermolecular interactions, for example, from high-order multipoles or weak CH···O hydrogen bonds, may have minor contributions to the local energy barrier against reorientating the molecules within the SAM.

2.3. C_{10}CHO SAMs Formed during AFM Nanografting. AFM-based nanografting was used to fabricate C_{10}CHO nanostructures, in which the SAM formation follows a completely different reaction pathway from that found during natural growth.[11,13,14] The results are summarized in Figure 7. Panel 7a shows an AFM topograph of a 400 × 400 nm^2 C_{10}CHO pattern fabricated into a C_{10}CHO matrix SAM grown at 296 K. The pattern was created by removing the matrix molecules with the AFM tip during scanning in a 1 mM C_{10}CHO solution, following a procedure described previously.[10−12] A high shaving force of 18 nN and a low scanning speed of 1 μm/s were used

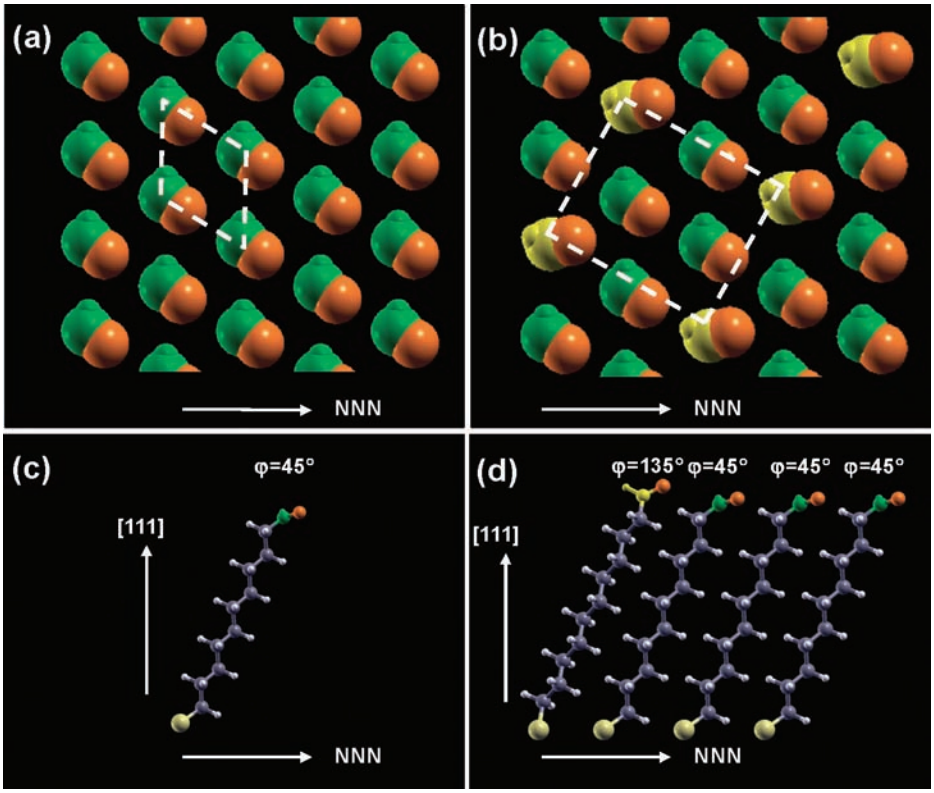

Figure 10. Proposed models for closely packed C_{10}CHO SAMs based on theoretical calculations (see text): the $(\sqrt{3}\times\sqrt{3})$R30° structure, in (a) top and (c) side views; the β-$c(4\times2)$ superstructure, in (b) top and (d) side views. For simplicity, the Au(111) surface is not shown, and only the CHO termini are displayed in the top views. The O atoms are displayed in orange; the C and H atoms in the CHO groups are represented in different colors for different twist angles. The CH_2 groups forming the alkyl chains are displayed in gray for all molecules in side views. The large atom at the bottom of the chains is the S atom. $\theta = 30°$ and $\chi = 0°$ for all molecules, while the φ angles are indicated in the diagrams. See text for a detailed discussion of backbone configurations and orientations of CHO termini.

for the fabrication of the nanopattern. Panel 7b is a higher magnification topograph of the area marked in Figure 7a. The images were acquired at a low imaging force, 0.5 nN, within 30 min after fabrication. No further changes in surface morphology were observed inside the patterned area during at least 3 h of subsequent imaging. The morphology of the matrix SAM [right side of Figure 7b] displays a much higher degree of heterogeneity (e.g., bright and dark contrasts) than the nanografted area, which appears smooth. Figure 7c shows the true height profile across regions indicated in panel 7b. The height profile inside the pattern [Figure 7b and c] suggests a homogeneous domain structure, with a height corrugation of 0.11 ± 0.02 nm. The similar heights of the nanopattern and of the tallest closely packed matrix domains indicate that both regions have similar coverage. The higher level of heterogeneity indicates the larger adsorbate mobility in the as-grown areas than in the nanografted regions. A proposed model is shown in Figure 7d, which illustrates the molecular packing inside and outside the nanografted area. The fact that near molecular-level mixing may be attained during nanografting suggests that the local molecule−molecule interaction is more significant upon adsorption than in solution phase, consistent with our calculation of dipole interactions among surface immobilized molecules.

3. The Molecular-Level Structure of C_{10}CHO SAMs in the Closely Packed Domains. The molecular-level structure of C_{10}CHO SAMs was investigated by high-resolution UHV-STM. Figure 8a−c shows high-resolution STM topographs of C_{10}CHO deposited at 296 K. At molecular level, the C_{10}CHO domains display almost exclusively the $(\sqrt{3}\times\sqrt{3})$R30° periodicity [Figure 8a and b]; that is, all molecules share the same (θ,χ,φ) orientations. The closely packed C_{10}CHO domains formed at 340 K or upon UHV annealing exhibit only $c(4 \times 2)$ superstructures, shown in Figure 9. The $(\sqrt{3}\times\sqrt{3})$R30° structure was not observed after annealing in either solution or UHV. This result is consistent with previous observations for methyl-terminated alkanethiols[26,40,57] and supports the conclusion that the $c(4\times2)$ structures of alkanethiols are thermodynamically more stable than the $(\sqrt{3}\times\sqrt{3})$R30°.

Another difference between CHO- and CH_3-terminated SAMs is the coverage of $c(4\times2)$ structures for as-grown monolayers. Domains displaying $c(4\times2)$ superstructures are only rarely encountered for CHO SAMs and are typically not more than 5 nm in size in Figure 8c. By comparison, the C_{11} SAMs formed at 296 K [Figure 8d] exhibit larger areas of $c(4\times2)$ superstructures, in addition to the $(\sqrt{3}\times\sqrt{3})$R30° domains. A large coverage of $c(4\times2)$ domains was also reported previously for as-deposited dodecanethiols.[24] The phase transition temperature is thus higher for C_{10}CHO SAMs than C_{11}, consistent with the stronger intermolecular interaction.

We studied in detail the adsorption of C_4CHO/Au(111) using DFT techniques, and all of the simulated $c(4\times2)$ structures were found energetically nearly degenerate with the most stable $(\sqrt{3}\times\sqrt{3})$R30° structures. A similar trend is observed for CH_3-terminated SAMs. Overall, the calculated energy difference between the two periodicities, ~1 kcal/mol, is consistent with previous DFT results of closely packed methylthiols[58−60] and decanethiols[61] adsorbed on Au(111), which predicted that the two adsorption models are energetically nearly degenerate within simulation accuracy. Alternative DFT calculation suggested that the formation of surface defects (adatoms or vacancies) may favor $c(4\times2)$ structures energetically.[60,62] In our DFT calculations, only defect-free Au surfaces were used. However, we note

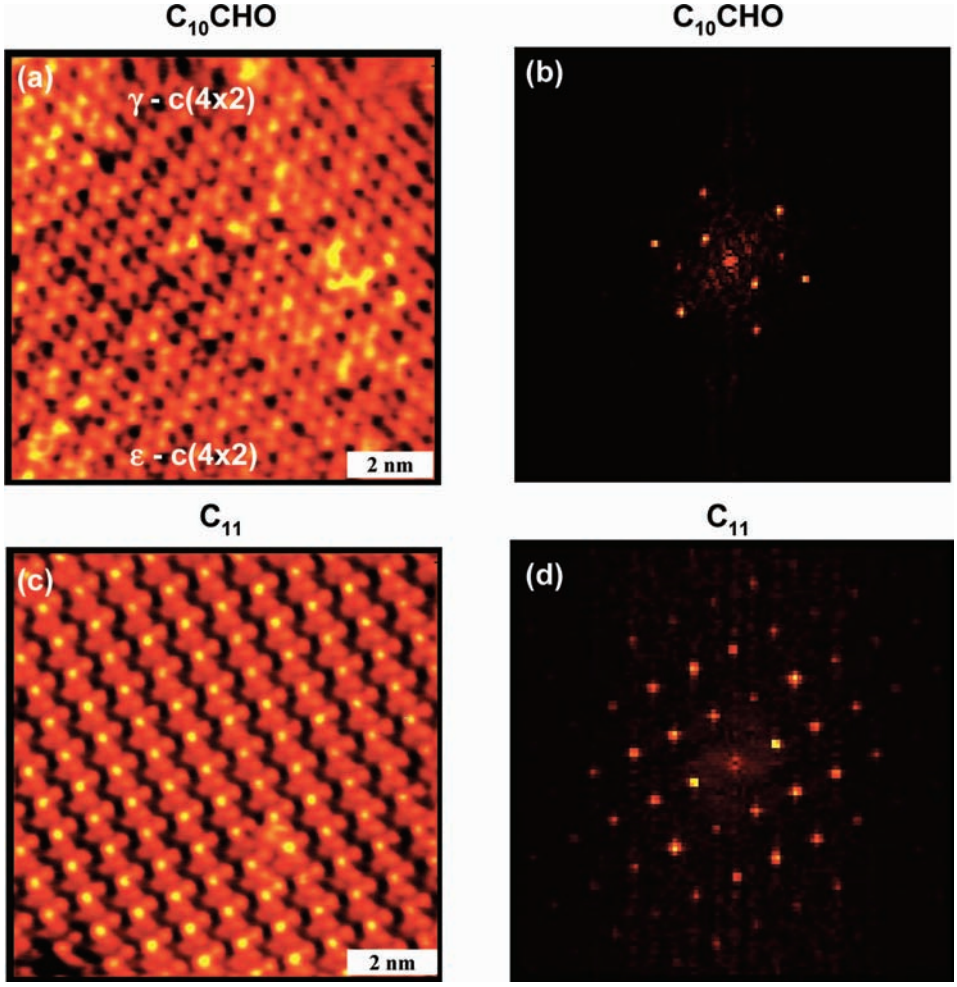

Figure 11. (a and b) High-resolution STM topograph and the corresponding FFT image of a $C_{10}CHO$ domain (two-dimensional crystal) formed at 340 K. Small regions displaying various types of periodicity are observed within the same closely packed domain (panel a), without being separated by domain boundaries or dislocations. The lack of long-range order in closely packed $C_{10}CHO$ domains is reflected by the disordered FFT pattern (panel b). (c and d) High-resolution STM topograph and the corresponding FFT image of a C_{11} domain after annealing at 345 K. Although defects are occasionally observed, the closely packed C_{11} domains display long-range order in (c), which is reflected by the numerous peaks in the FFT pattern in (d). The images were acquired at (a) (0.8 V, 9 pA), and (c) (0.8 V, 16 pA).

that vdW interactions are not fully captured in the current DFT/GGA level. For alkanethiols/Au(111), the characteristic interaction energy between neighboring chains is estimated to be about 2 kcal/mol for each CH_2 group in the alkyl chain. For a chain length of $n = 11$, as studied in the current STM experiments, the difference of vdW interaction energies should reveal the detailed relative orientations among hydrocarbon chain in the two proposed models.

The observation of adjacent domains displaying different $c(4\times2)$ contrasts at the same imaging conditions [Figure 9a and b] indicates that these domains are composed of structurally different phases; that is, they are characterized by different (θ,χ,φ) combinations.[28,30] $C_{10}CHO$ SAMs formed at 340 K exhibited regions showing ϵ, γ, and δ-$c(4\times2)$.[24,63,64] The highest population phase for UHV annealed SAMs was the β-$c(4\times2)$ [Figure 9d], but a high coverage of γ-$c(4\times2)$ [Figure 9e] and δ-$c(4\times2)$ [Figure 9f] was also observed.[24,63,64] The β, δ, and γ-$c(4\times2)$ superstructures are also the most commonly observed $c(4\times2)$ structures on annealed methyl-terminated alkanethiol SAMs.[26,27,57,63,64] The structure shown in Figure 9h, denominated here as φ-$c(4\times2)$, has not been reported previously and was observed in our experiments on only one sample. It is likely that this contrast corresponds to a rare and metastable phase.

In Figure 10, we constructed structure models for $(\sqrt{3}\times\sqrt{3})$-R30° and $c(4\times2)$ structures, based on the structure predicted by molecular dynamics for alkanethiol chain orientations[28] and our DFT calculation to determine the terminal aldehyde orientations. The construction of structural models directly from the high-resolution structures revealed by STM is still difficult. Electronic effects contributing to the STM topograph may complicate the determination of the true physical surface structures.[26] The model in Figure 10b represents the most frequently observed phase, that is, the β-$c(4\times2)$. For clarity, only the aldehyde groups are shown in the top view, displayed in different colors for the four nonequivalent molecules in the unit cell. There are 4 chains per unit cell (3-1 mode), with the (θ,χ,φ) angles indicated in Figure 10.[28] The CHO orientations are based on DFT results of the C_4CHO/Au(111) systems, assuming that the chain length dependence is weak within this range ($n < 12$). The C═O bonds lie nearly parallel to the surface, as determined by the balance between intramolecular (CHO rotation with respect to alkane backbone) and intermolecular (dipole−dipole) energies. The model accounts for the $c(4\times2)$ periodicity, and also another observation in STM images shown in Figure 9; that is, some $C_{10}CHO$ molecules appear in the STM topographs as spots slightly elongated along NN or

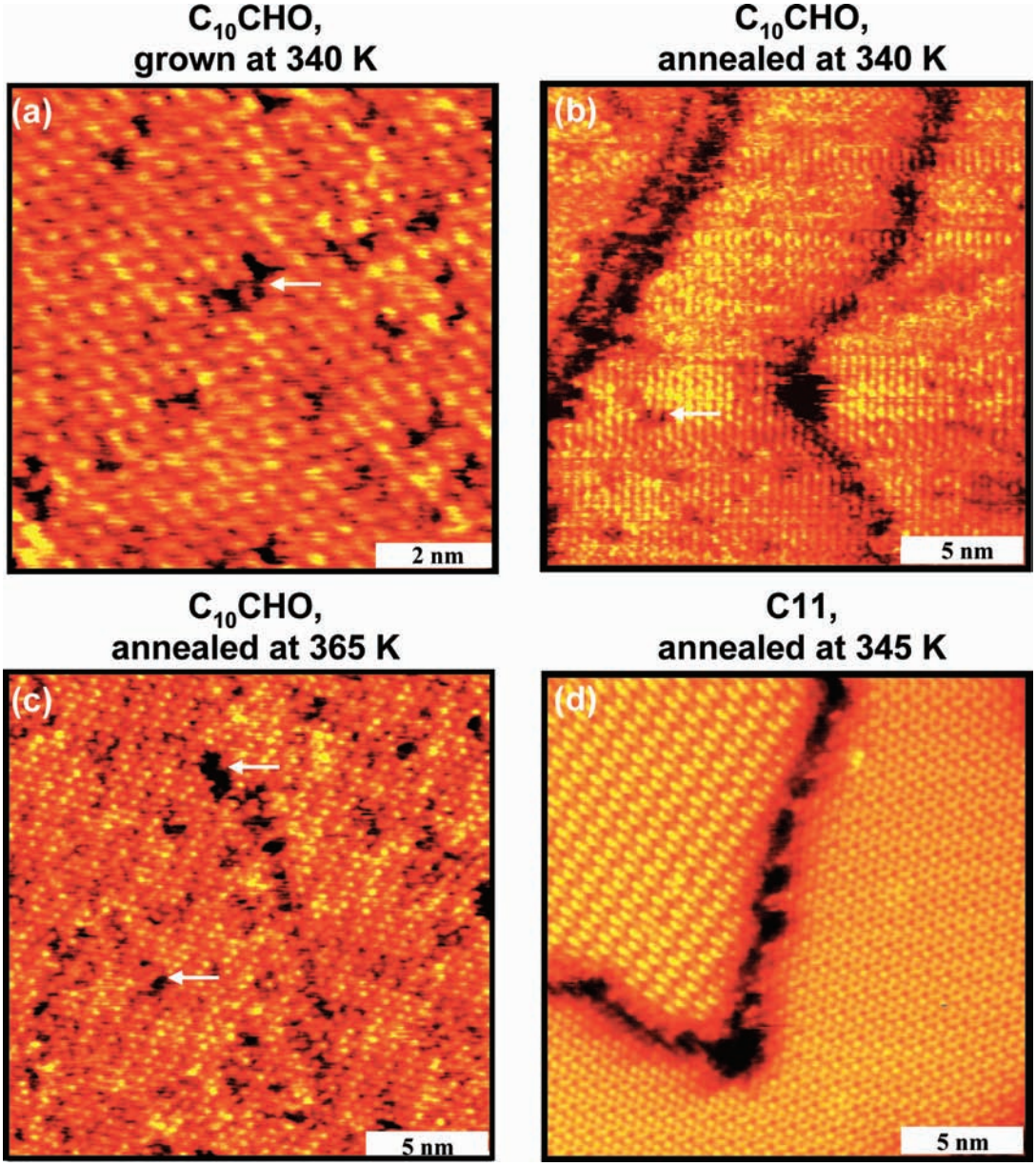

Figure 12. (a−c) High-resolution STM topographs of $C_{10}CHO$ SAMs prepared by various methods, showing a high density of missing molecules within the closely packed domains. (d) High-resolution STM topograph of annealed C_{11}, showing well-ordered closely packed domains with no missing molecules. The images were acquired at (a) (0.8 V, 2 pA), (b) (1.3 V, 20 pA), (c) (0.3 V, 5 pA), and (d) (0.8 V, 16 pA).

NNN directions. These elongated spots may correspond to aldehyde groups having the C═O bond oriented nearly parallel to the substrate.

4. Phase Defects in Closely Packed $C_{10}CHO$ Domains. A unique observation is that the $C_{10}CHO$ closely packed domains often contain phase defects. Specifically, the STM contrast varies within the same ordered domains, where there are no domain boundaries, line defects, or dislocations. This is exemplified in Figure 11a for a closely packed domain formed at 340 K. The corresponding FFT image [Figure 11b] shows only several weak peaks near the origin, indicating a low degree of long-range order. In contrast, C_{11} SAMs exhibit a high degree of long-range order within two-dimensional crystals (see Figure 11).[26,40] These phase defects may originate from the variations in the orientations either of the CHO termini or of the alkyl chains within this domain. Becase variations in (θ,χ,φ) within the closely packed domains are difficult due to steric constrains,[1] the first hypothesis is more plausible. If one compares the energy barrier, the rotation of termini CHO is calculated to be at least 2.5 kcal/mol higher than rotation of the three H-atoms in the methyl terminal groups. It is possible that the rotational hindrance present in CHO SAMs enables STM to capture those phase defects.

Another type of phase defect in $C_{10}CHO$ SAMs is revealed in high-resolution STM images (Figure 12), that is, missing molecules. A high density of missing molecules within domains of closely packed $C_{10}CHO$ molecules is observed for both as-deposited [Figures 8a,b, 9a, and 12a] and UHV-annealed [Figures 9b, 12b,c] monolayers. This finding is unusual especially for alkanethiol SAMs formed at elevated temperatures or upon annealing in UHV.[26,40] For SAMs without polar termini, the high surface mobility, which results in an increase in domain size and long-range order, also facilitates the healing of point defects. For example, C_{11} SAMs annealed within the same temperature range exhibit closely packed domains, which appear nearly defect-free (Figure 12d). The presence of a high density of point defects in closely packed $C_{10}CHO$ domains, especially after annealing, is consistent with our previous discussion

regarding the strong dipole−dipole interactions, which hinder the movement of individual molecules and manifest into point defects in the high coverage regions.

Conclusions

We present the first high-resolution UHV-STM and AFM study of aldehyde-terminated alkanethiol SAMs. At molecular level, closely packed C_{10}CHO domains formed at room temperature exhibit mostly $(\sqrt{3}\times\sqrt{3})$R30° periodicity, while several $c(4\times2)$ superstructures were observed for SAMs formed at elevated temperatures or upon UHV annealing. This result supports the conclusion that the $c(4\times2)$ structures of functional alkanethiols are thermodynamically more stable than the $(\sqrt{3}\times\sqrt{3})$R30°. Based on the energetics from the DFT calculations, the CHO termini in the $(\sqrt{3}\times\sqrt{3})$R30° and $c(4\times2)$ structures are approximately parallel to the surface to optimize the dipole−dipole interactions. Phase defects were captured in STM images, indicating the variation in termini orientation and missing molecules within the same ordered domains.

At nanometer level, C_{10}CHO SAMs exhibit a higher degree of heterogeneity in comparison to their *n*-alkanethiol counter part, for example, C_{11} SAMs. Disordered regions are clearly visible under both STM and AFM, and the ordered domains are much smaller than C_{11} SAMs. These results are consistent with the presence of strong intermolecular interactions, mostly dipole−dipole interactions among the neighboring aldehyde termini, which hinder the movement of the molecules and reorientation of the chain. This explanation is supported by the structural study of C_{10}CHO SAMs under elevated temperatures and upon thermo-annealing in UHV, where the input of thermal energy is not sufficient to overcome the barrier to form long-range order at high temperatures and reduced coverages. The detailed structural information on C_{10}CHO SAMs at nanometer and molecular scale is important toward the understanding of the force balance in SAM formation, and their applications in the immobilization of biomolecules such as protein. Work is in progress to dissect contributions of all interactions in further detail to understand the SAM structure toward further realizing their applications.

Acknowledgment. This work was supported by the University of California, Davis, a Development Award from UC Davis Cancer Center, National Institutes of Health (R21-GM077850), DOE/BES (DE-FG02-06ER46262), and a seed fund from CPIMA via Stanford University (NSF-MRSEC DMR-0213618). We thank Mr. Christopher Fleming and Ms. Susan G. Stagner at University of California, Davis, for helpful discussions. Some of the DFT calculations were performed at NERSC and SDSC facilities.

References and Notes

(1) Schreiber, F. *Prog. Surf. Sci.* **2000**, *65*, 151.
(2) Mrksich, M.; Chen, C. S.; Xia, Y. N.; Dike, L. E.; Ingber, D. E.; Whitesides, G. M. *Proc. Natl. Acad. Sci. U.S.A.* **1996**, *93*, 10775.
(3) Liu, G. Y.; Amro, N. A. *Proc. Natl. Acad. Sci. U.S.A.* **2002**, *99*, 5165.
(4) Wadu-Mesthrige, K.; Amro, N. A.; Liu, G. Y. *Scanning* **2000**, *22*, 380.
(5) Wadu-Mesthrige, K.; Amro, N. A.; Garno, J. C.; Xu, S.; Liu, G. Y. *Biophys. J.* **2001**, *80*, 1891.
(6) Li, X. L.; He, J.; Hihath, J.; Xu, B. Q.; Lindsay, S. M.; Tao, N. J. *J. Am. Chem. Soc.* **2006**, *128*, 2135.
(7) Tour, J. M. *Acc. Chem. Res.* **2000**, *33*, 791.
(8) McCreery, R. L. *Chem. Mater.* **2004**, *16*, 4477.
(9) Joachim, C.; Gimzewski, J. K.; Aviram, A. *Nature* **2000**, *408*, 541.
(10) Liu, G. Y.; Xu, S. *Abstr. Pap.-Am. Chem. Soc.* **1997**, *214*, 29.
(11) Xu, S.; Laibinis, P. E.; Liu, G. Y. *J. Am. Chem. Soc.* **1998**, *120*, 9356.
(12) Liu, J. F.; Cruchon-Dupeyrat, S.; Garno, J. C.; Frommer, J.; Liu, G. Y. *Nano Lett.* **2002**, *2*, 937.
(13) Yu, J. J.; Tan, Y. H.; Li, X.; Kuo, P. K.; Liu, G. Y. *J. Am. Chem. Soc.* **2006**, *128*, 11574.
(14) Ryu, S.; Schatz, G. C. *J. Am. Chem. Soc.* **2006**, *128*, 11563.
(15) Amro, N. A.; Xu, S.; Liu, G. y. *Langmuir* **2000**, *16*, 3006.
(16) Crooks, R. M.; Ricco, A. J. *Acc. Chem. Res.* **1998**, *31*, 219.
(17) Flink, S.; van Veggel, F.; Reinhoudt, D. N. *Adv. Mater.* **2000**, *12*, 1315.
(18) Willner, I.; Katz, E. *Angew. Chem., Int. Ed.* **2000**, *39*, 1180.
(19) Li, L.; Chen, S.; Jiang, S. *Langmuir* **2003**, *19*, 2974.
(20) Klare, J. E.; Tulevski, G. S.; Nuckolls, C. *Langmuir* **2004**, *20*, 10068.
(21) Rozkiewicz, D. I.; Kraan, Y.; Werten, M. W. T.; de Wolf, F. A.; Subramaniam, V.; Ravoo, B. J.; Reinhoudt, D. N. *Chem.-Eur. J.* **2006**, *12*, 6290.
(22) Dannenberger, O.; Weiss, K.; Himmel, H.-J.; Jager, B.; Buck, M.; Woll, C. *Thin Solid Films* **1997**, *307*, 183.
(23) Sushko, M. L.; Shluger, A. L. *J. Phys. Chem. B* **2007**, *111*, 4019.
(24) Delamarche, E.; Michel, B.; Gerber, C.; Anselmetti, D.; Guntherodt, H. J.; Wolf, H.; Ringsdorf, H. *Langmuir* **1994**, *10*, 2869.
(25) Delamarche, E.; Michel, B.; Biebuyck, H. A.; Gerber, C. *Adv. Mater.* **1996**, *8*, 719.
(26) Riposan, A.; Liu, G.-y. *J. Phys. Chem. B* **2006**, *110*, 23926.
(27) Poirier, G. E.; Tarlov, M. J. *Langmuir* **1994**, *10*, 2853.
(28) Li, T. W.; Chao, I.; Tao, Y. T. *J. Phys. Chem. B* **1998**, *102*, 2935.
(29) Fenter, P.; Eberhardt, A.; Liang, K. S.; Eisenberger, P. *J. Chem. Phys.* **1997**, *106*, 1600.
(30) Pertsin, A. J.; Grunze, M. *Langmuir* **1994**, *10*, 3668.
(31) Nuzzo, R. G.; Korenic, E. M.; Dubois, L. H. *J. Chem. Phys.* **1990**, *93*, 767.
(32) Nuzzo, R. G.; Dubois, L. H.; Allara, D. L. *J. Am. Chem. Soc.* **1990**, *112*, 558.
(33) Ito, E.; Konno, K.; Noh, J.; Kanai, K.; Ouchi, Y.; Seki, K.; Hara, M. *Appl. Surf. Sci. 12th Int. Conf. Solid Film Surf.* **2005**, *244*, 584.
(34) Poirier, G. E.; Pylant, E. D.; White, J. M. *J. Chem. Phys.* **1996**, *104*, 7325.
(35) Hyun, M.; Rhee, C. K. *Bull. Korean Chem. Soc.* **2001**, *22*, 213.
(36) Rhee, C. K.; Kim, Y. N. *Appl. Surf. Sci.* **2004**, *228*, 313.
(37) Sawaguchi, T.; Sato, Y.; Mizutani, F. *J. Electroanal. Chem.* **2001**, *507*, 256.
(38) *Handbook of Chemistry and Physics*, 87th ed.; Lide, D. R., Ed.; CRC Press Inc.: New York, 2006.
(39) Ishida, T.; Yamamoto, S.; Mizutani, W.; Motomatsu, M.; Tokumoto, H.; Hokari, H.; Azehara, H.; Fujihira, M. *Langmuir* **1997**, *13*, 3261.
(40) Yang, G. H.; Liu, G. Y. *J. Phys. Chem. B* **2003**, *107*, 8746.
(41) Perdew, J. P.; Burke, K.; Ernzerhof, M. *Phys. Rev. Lett.* **1996**, *77*, 3865.
(42) Baroni, S.; Dal Corso, A.; de Gironcoli, S.; Giannozzi, P.; Cavazzoni, C.; Ballabio, G.; Scandolo, S.; Chiarotti, G.; Focher, P.; Pasquarello, A.; Laasonen, K.; Trave, A.; Car, R.; Marzari, N.; Kokalj, A., http://www.pwscf.org.
(43) Li, Y.; Lu, D.; Swanson, S. A.; Scott, J. C.; Galli, G., submitted.
(44) Monkhorst, H. J.; Pack, J. D. *Phys. Rev. B* **1976**, *13*, 5188 LP.
(45) Castronovo, M.; Bano, F.; Raugei, S.; Scaini, D.; Dell'Angela, M.; Hudej, R.; Casalis, L.; Scoles, G. *J. Am. Chem. Soc.* **2007**, *129*, 2636.
(46) Jourdan, J. S.; Cruchon-Dupeyrat, S. J.; Huan, Y.; Kuo, P. K.; Liu, G. Y. *Langmuir* **1999**, *15*, 6495.
(47) Qian, Y. L.; Yang, G. H.; Yu, J. J.; Jung, T. A.; Liu, G. Y. *Langmuir* **2003**, *19*, 6056.
(48) Gordon, A. J. a. F., R. A. *The Chemist's Companion: A Handbook of Practical Data, Techniques and References*; John Wiley & Sons: New York, 2006.
(49) Sprik, M.; Delamarche, E.; Michel, B.; Rothlisberger, U.; Klein, M. L.; Wolf, H.; Ringsdorf, H. *Langmuir* **1994**, *10*, 4116.
(50) Song, X.; Sylvain, J. N. C.-D.; Jayne, C. G.; Gang-Yu, L.; Jennings, G. K.; Tseh-Hwan, Y.; Paul, E. L. *J. Chem. Phys.* **1998**, *108*, 5002.
(51) Li, L.; Chen, S.; Jiang, S. *Langmuir* **2003**, *19*, 3266.
(52) Poirier, G. E.; Pylant, E. D. *Science* **1996**, *272*, 1145.
(53) Staub, R.; Toerker, M.; Fritz, T.; Schmitz-Hubsch, T.; Sellam, F.; Leo, K. *Langmuir* **1998**, *14*, 6693.
(54) Poirier, G. E. *Langmuir* **1999**, *15*, 1167.
(55) Poirier, G. E.; Fitts, W. P.; White, J. M. *Langmuir* **2001**, *17*, 1176.
(56) Tsukamoto, K.; Kubo, T.; Nozoye, H. *Appl. Surf. Sci.* **2005**, *244*, 578.
(57) Delamarche, E.; Michel, B.; Kang, H.; Gerber, C. *Langmuir* **1994**, *10*, 4103.
(58) Vargas, M. C.; Giannozzi, P.; Selloni, A.; Scoles, G. *J. Phys. Chem. B* **2001**, *105*, 9509.

(59) Morikawa, Y.; Hayashi, T.; Liew, C. C.; Nozoye, H. *Surf. Sci.* **2002**, *507*, 46.
(60) Morikawa, Y.; Liew, C. C.; Nozoye, H. *Surf. Sci.* **2002**, *514*, 389.
(61) Fischer, D.; Curioni, A.; Andreoni, W. *Langmuir* **2003**, *19*, 3567.
(62) Wang, J. g.; Selloni, A. *J. Phys. Chem. C* **2007**, *111*, 12149.
(63) Lussem, B.; Muller-Meskamp, L.; Karthauser, S.; Waser, R. *Langmuir* **2005**, *21*, 5256.
(64) Fukuma, T.; Ichii, T.; Kobayashi, K.; Yamada, H.; Matsushige, K. *J. Appl. Phys.* **2004**, *95*, 1222.